2022-01-0384

# Advanced Turbulence Model for SI Combustion in a Heavy-Duty NG Engine

**Author, co-author (Do NOT enter this information. It will be pulled from participant tab in MyTechZone)**

Affiliation (Do NOT enter this information. It will be pulled from participant tab in MyTechZone)

## Abstract

In the recent years, the interest in heavy-duty engines fueled with Compressed Natural Gas (CNG) is increasing due to the necessity to comply with the stringent $CO_2$ limitation imposed by national and international regulations. Indeed, the reduced number of carbon atoms of the NG molecule allows to reduce the $CO_2$ emissions compared to a conventional fuel. The possibility to produce synthetic methane from renewable energy sources, or bio-methane from agricultural biomass and/or animal waste, contributes to support the switch from conventional liquid fuels to CNG.

To drive the engine development and reduce the time-to-market, the employment of numerical analysis is mandatory. This requires a continuous improvement of the simulation models toward real predictive analyses able to reduce the experimental R&D efforts.

In this framework, 1D numerical codes are fundamental tools for system design, energy management optimization, and so on. The present work is focused on the improvement of the turbulence sub-model, originally conceived to describe turbulence evolution in tumble-promoting engines.

The turbulence model is here developed with reference to a SI heavy-duty CNG engine derived from a diesel engine. In this architecture, due to the flat cylinder head, turbulence is generated primarily by swirl and squish flow motions unlike conventional tumble-assisted SI engines.

To extend the turbulence model, a 3D simulation campaign was carried out aiming at extracting the information for model conceptualization and validation.

The turbulence sub-model demonstrated to properly predict turbulence and swirl/tumble evolution under various operating conditions, without the need for any case-dependent tuning. It hence presented the potential for appropriately support the predictive capabilities of any combustion model for SI heavy-duty tumble- and swirl-promoting engines.

## Introduction

The worldwide transport system is facing an extraordinary evolution never seen before, with a well-defined target: the phase-out from carbon fossil fuels as soon as possible. In particular, the EU target by 2050 for the transport sector is a complete $CO_2$ emission-free energy supply, together with a fully “clean” mobility [1]

Currently around 99.8% of transport is powered by combustion engines and around 95% of transport energy is provided by petroleum- based liquid fuels; every alternative starts from a low base and faces very significant barriers to unlimited expansion. Hence, even by 2040, 85–90% of transport energy is expected to be provided by conventional fuels powering combustion engines. It is imperative that the performance of such engines is improved in terms of efficiency and exhaust pollutants if current greenhouse gas emission targets are to be achieved [2].

Regarding Heavy-Duty (HD) commercial vehicles, the Compressed and Liquefied Natural Gas (CNG and LNG) nowadays, and the bio-methane (bio-NG) and the Power-To-Gas methane (PTG) in the future, represent high potential co-solutions to match the mid-term and long-term neutral climate targets [3, 4, 5].

In this scenario, it is essential to keep the costs of engine development affordable. For this reason, companies, but also researchers, use powerful software tools synergically with experimental study. In this perspective, it is important to have mathematical equations that can describe the different phenomenologies.

The aim of this work is to make an additional contribution to the class of the turbulence phenomenological models, aiming at describing the turbulence and mean flow evolutions within the cylinder of an ICE.

The turbulent and mean flow fields inside the cylinder play a major role in Spark Ignition (SI) engines. Multiple phenomena that occur during the high pressure part of the engine cycle, such as early flame kernel development, flame propagation and gas-to-wall heat transfer, are influenced by in-cylinder turbulence.

Turbulence inside the cylinder is primarily generated via high shear flows that occur during the intake process, via high velocity injection sprays and by the destruction of macro-scale motions produced by tumbling and/or swirling structures before Top Dead Center (TDC).

It is generally recognized that tumble motion contributes to the enhancement of combustion in SI engines. The tumble motion decays when the piston is close to the TDC, increasing the Turbulent Kinetic Energy (TKE).

CNG SI HD commercial vehicles commonly derive from diesel Compression Ignition (CI) engines in terms of cylinder head and combustion chamber geometry [6]. In the case of a flat cylinder head with a bowl piston, tumble and swirl are both fundamentals to the turbulent motion field characterization, and also the squish plays an important role, especially around the TDC. Swirl, tumble and squish flows enhance turbulence intensity during late compression by

breaking down these flows to small scale turbulent eddies. This provides increase of turbulent flame speed and an acceleration of burning rate [7].

In a 0D environment, most of in-cylinder flow models found in the literature follows a *K-k* energy cascade approach or a *k-ε* approach, where *K* and *k* are the mean and turbulent kinetic energy, respectively, and *ε* is the turbulent dissipation rate. One of the first 0D flow models in which the swirl motion is contemplated, was the *k-ε* model of Borgnakke et al. [8]. In this work the swirl motion was modeled as a macro vortex undergoing solid body rotation. Morel et al. [9] proposed a *k-ε* model in which both swirl and squish motions affected the heat transfer in a bowl-in-piston combustion chamber. The above works presented a *k-ε* model in which the 0D equations of TKE, *k*, and dissipation rate, *ε*, are derived from 3D models. A different approach is to analyze the energy cascade mechanism that occurs from mean flow field to turbulent flow field, commonly labelled as *K-k* model. In [10] Grasreiner et al. developed a model in which TKE is generated by tumble and swirl dissipation, with a focus on the decay functions for different types of charge motion. Fogla et al. [11] defined a more comprehensive approach, where the *K-k* and *k-ε* models are synthesized in a so-called *K-k-ε*, taking into account the energy cascade mechanism and dissipation rate description together.

Authors have made significant improvements to the *K-k* family of models [12, 13, 14], especially in terms of accounting for the effects of tumble motion and variable valve lift/timings. In [15] the authors have widened the study, defining an advanced model that represents an extension of a conventional two-equations *K-k* formulation, where the tumble and dissipation rate equations are added, leading to a *K-k-T* model, where *T* is specific angular momentum associated to the tumble motion.

In SI engines, the efforts were directed mainly to develop flow models that account for the tumble effects on turbulent kinetic energy. For the above-mentioned reasons, authors felt the need to develop a 0D model that takes into account all the charge motions involved into the turbulence generation near the TDC, including tumble, and swirl and squish motions. This work is a further advance of the aforementioned *K-k-T* model [15], with an additional equation for the angular momentum associated to the swirl motion, leading to a *K-k-T-S* model.

The paper is organized as follows. The next section presents the governing equations of the flow model. That is followed by the description of the engine geometry and the setup of 3D-CFD runs that were used to calibrate and validate the proposed model. The Results and Discussion section presents the comparison between the predictions of the 0D model and the results of 3D-CFD simulations. The final section presents some conclusions of the current study and directions for future investigations.

## 0D In-Cylinder flow model

The following pattern of turbulence is a further step forward to the previous work of the authors [15]. The turbulence model presented in that work was one of the *K-k* family, but based on 3 equations, one for the kinetic energy associated with the mean flow *K*, one for the kinetic energy of the turbulent motion field flow *k* and one for the specific angular momentum *T* of the tumble motion. This model, *K-k-T*, is strongly indicated for all those classes of tumble-assisted SI engines.

In this work, the engine under consideration has a cylinder head derived from a diesel engine. Hence, during the intake stroke, there is mainly an ordered motion of swirl rather than tumble.

For a question of completeness, the complete model will be presented, including the equations of the previous work of authors [15], with the addition of the swirl momentum equation:

$$\frac{\boldsymbol{dmK}}{\boldsymbol{dt}} = (\dot{\boldsymbol{m}}\boldsymbol{K})_{\boldsymbol{inc}} - (\dot{\boldsymbol{m}}\boldsymbol{K})_{\boldsymbol{out}} - \frac{\boldsymbol{dmK_T}}{\boldsymbol{dt}} - \frac{\boldsymbol{dmK_S}}{\boldsymbol{dt}} + \boldsymbol{mK}\frac{\dot{\boldsymbol{\rho}}}{\boldsymbol{\rho}} - \boldsymbol{P} + \dot{\boldsymbol{K}}_{\boldsymbol{inj}} \quad (1)$$

$$\frac{\boldsymbol{dmk}}{\boldsymbol{dt}} = (\dot{\boldsymbol{m}}\boldsymbol{k})_{\boldsymbol{inc}} - (\dot{\boldsymbol{m}}\boldsymbol{k})_{\boldsymbol{out}} + \frac{\boldsymbol{2}}{\boldsymbol{3}}\frac{\dot{\boldsymbol{\rho}}}{\boldsymbol{\rho}}\left(-\boldsymbol{m}\boldsymbol{v}_{\boldsymbol{t}}\frac{\dot{\boldsymbol{\rho}}}{\boldsymbol{\rho}} + \boldsymbol{mk}\right) + \boldsymbol{P} - \boldsymbol{m\varepsilon} \quad (2)$$

$$\frac{\boldsymbol{dmT}}{\boldsymbol{dt}} = (\dot{\boldsymbol{m}}\boldsymbol{T})_{\boldsymbol{inc}} - (\dot{\boldsymbol{m}}\boldsymbol{T})_{\boldsymbol{out}} - \boldsymbol{f}_{\boldsymbol{dT}}\frac{\boldsymbol{mT}}{\boldsymbol{t_T}} \quad (3)$$

$$\frac{\boldsymbol{dmS}}{\boldsymbol{dt}} = (\dot{\boldsymbol{m}}\boldsymbol{S})_{\boldsymbol{inc}} - (\dot{\boldsymbol{m}}\boldsymbol{S})_{\boldsymbol{out}} - \boldsymbol{f}_{\boldsymbol{dS}}\frac{\boldsymbol{mS}}{\boldsymbol{t_S}} \quad (4)$$

The equations shown above govern the evolution of the following flow quantities:

1. Mean kinetic energy $\boldsymbol{K} = (\boldsymbol{1/2})\boldsymbol{U^2}$, where *U* is the mean velocity inside the cylinder.
2. $\frac{\boldsymbol{dmK_T}}{\boldsymbol{dt}} = \frac{\boldsymbol{U_T}}{\boldsymbol{r_T}}\left(\boldsymbol{f}_{\boldsymbol{dT}}\frac{\boldsymbol{mT}}{\boldsymbol{t_T}}\right)$ is the kinetic energy destruction associated to the tumble flow inside the cylinder.
3. $\frac{\boldsymbol{dmK_S}}{\boldsymbol{dt}} = \frac{\boldsymbol{U_S}}{\boldsymbol{r_S}}\left(\boldsymbol{f}_{\boldsymbol{dS}}\frac{\boldsymbol{mS}}{\boldsymbol{t_S}}\right)$ is the kinetic energy destruction associated to the swirl flow inside the cylinder.
4. Turbulent kinetic energy $\boldsymbol{k} = (\boldsymbol{3/2})\boldsymbol{u'^2}$, where *u'* is the intensity of the turbulent field inside the cylinder, assumed to be homogeneous and isotropic.
5. Specific angular momentum of the tumble motion $\boldsymbol{T} = \boldsymbol{U_T r_T}$, where $U_T$ is the tumble vortex velocity and $r_T$ is the tumble radius. Tumble speed is commonly expressed in a non-dimensional form as tumble number $\boldsymbol{N_T} = \boldsymbol{U_T}/(\boldsymbol{\omega_{eng} r_T})$, being $\boldsymbol{\omega_{eng}}$ the engine angular speed.
6. Specific angular momentum of the swirl motion $\boldsymbol{S} = \boldsymbol{U_S r_S}$, where $U_S$ is the swirl vortex velocity and $r_S$ is the swirl radius. As well as tumble number, swirl number is defined as: $\boldsymbol{N_S} = \boldsymbol{U_S}/(\boldsymbol{\omega_{eng} r_S})$.

The term *m* multiplying the flow quantities is the in-cylinder mass, $\dot{K}_{inj}$ is the kinetic energy associated to in-cylinder fuel injection.

**Convective flows** – The first and the second term in the above equations describe incoming and outcoming convective flows through the valves. The following relations are used:

$$(\dot{m}K)_{inc} = \frac{1}{2}\left[\dot{m}_{inf}\left(c_{Kin0}v_{Kinf}\right)^2 + \dot{m}_{exf}v_{Kexf}^2 + \dot{m}_{exb}v_{Kexb}^2\right] \quad (5)$$

$$(\dot{m}K)_{out} = K(\dot{m}_{inb} + \dot{m}_{exf}) \quad (6)$$

$$(\dot{m}k)_{inc} = 0 \quad (7)$$

$$(\dot{m}k)_{out} = k(\dot{m}_{inb} + \dot{m}_{exf}) \quad (8)$$

$$(\dot{m}T)_{inc} = r_T\left(\dot{m}_{inf}c_{Tin0}v_{Tinf} - \dot{m}_{exf}v_{Texf} - \dot{m}_{exb}v_{Texb}\right) \quad (9)$$

$$(\dot{m}T)_{out} = T\,(\dot{m}_{inb} + \dot{m}_{exf}) \quad (10)$$

$$(\dot{m}S)_{inc} = r_S(\dot{m}_{inf}c_{Sin}v_{Sinf} - \dot{m}_{exf}c_{Sex}v_{Sexf} - \dot{m}_{exb}v_{Sexb}) \quad (11)$$

$$(\dot{m}S)_{out} = S\,(\dot{m}_{inb} + \dot{m}_{exf}) \quad (12)$$

In the Equations above $\dot{m}_{in}$ and $\dot{m}_{ex}$ indicate the mass flow entering and exiting the cylinder through the valves, respectively. The subscripts *f* and *b* indicate the directions of the flow through the valves, that is forward and backward.

In the Equations 5, 9 and 11 the velocities $v_K$, $v_T$ and $v_S$ include the flow losses through the valves, comprising the discharge, the tumble and the swirl coefficients, respectively.

The multipliers $c_{Kin0}$, $c_{Tin0}$, $c_{Sin}$ and $c_{Sex}$ permit to tune the discharge, the tumble and the swirl coefficients. As seen in a previous authors' work [12], the intake port inclination influences the tumble velocity inside the cylinder. A larger inclination determines higher velocities of the flow passing through the intake valve, causing a more intense tumble vortex during the intake. In the present work, the SI engine under study is derived from a diesel one, so the intake runners are designed to produce more swirl than tumble. In Equation 5, in addition to the contributions of fluxes entering the cylinder (first and third terms), also the effects of flux exiting the cylinder through the exhaust valve are considered (second term). This last contribution takes into account the local flow acceleration to which a portion of cylinder charge is subjected due to the outcoming flow.

The last two terms of the Equations 9 and 11 give a subtractive contribution considering the reverse tumble and swirl that could destroy the two ordered motions.

**Decay functions** – In the system of Equations 1-4, the terms $f_{dT}\frac{mT}{t_T}$ and $f_{dS}\frac{mS}{t_S}$ express the decay of the two main ordered motions due to the shear stresses with the combustion chamber walls. A decay function $f_d$ is used for the tumble and another one for the swirl, considering a characteristic time scale $t_T$ for the tumble and $t_S$ for the swirl.

$$f_{dT} = c_{fd0,T} + c_{fdm,T}\left[\max\left(\frac{B}{H},1\right) - 1\right] \quad (13)$$

$$t_T = \frac{r_T}{u'} \quad (14)$$

$$f_{dS} = c_{fd0,S} + c_{fdm,S}\left|\frac{U_{sq}}{U_S}\right| \quad (15)$$

$$t_S = \frac{r_S}{u'} \quad (16)$$

The two decay functions for tumble and swirl are similar, both dependent on a constant term, and on a time-varying term. The former considers the dissipation of the ordered motions due to internal viscous forces and it is active for all the engine cycle, the latter adjusts the dissipation effects due to the piston rising (Figure 1 and Figure 2). More specifically, the second term of tumble decay describes its characteristic collapse due to piston rising, and it is inversely related to the piston position, *H*, normalized by the cylinder bore, *B* (see Figure 1). The second term of swirl decay mimics the progressive destroy of swirl motion when this interacts with squish motion during the compression stroke, and it is assumed proportional to the ratio between the squish velocity, $U_{sq}$, and the swirl velocity. To modulate the two contributions to tumble and swirl decays, for each of those, two parameters $c_{fd0,x}$ and $c_{fdm,x}$ are introduced in Equations 13 and 15. The characteristic time scales, $t_T$ and $t_S$, in Equations 14 and 16 are related to the tumble and swirl radius, respectively, and those are explained by the Equations 17-18.

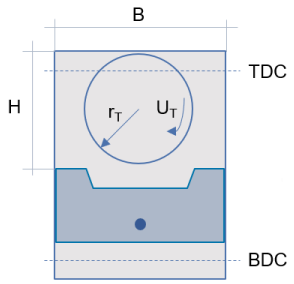


Figure 1 - Qualitative sketch of the tumble vortex.

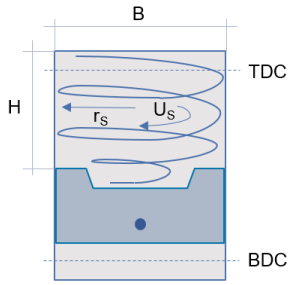


Figure 2 - Qualitative sketch of the swirl vortex.

$$r_{T,S} = c_{r0T,S} + c_{rmT,S}\frac{1}{4}\sqrt{B_\vartheta^2 + (H + s_{bowl})^2} \quad (17)$$

$$B_\vartheta = \frac{(V_{cyl} - V_{bowl})\cdot B + V_{bowl}\cdot d_{bowl}}{V_{cyl}} \quad (18)$$

In the Equation 17, $B_\theta$ and $(H+s_{bowl})$ are instantaneous representative dimensions, along cylinder radial and axial directions, around which develop ordered motions, while $c_{r0T}$ and $c_{rmT}$ (or $c_{r0S}$ and $c_{rmS}$) are two parameters that allow to adjust the tumble (or swirl) radius. $s_{bowl}$ is the piston bowl height (Figure 3). In the Equation 18, $V_{cyl}$ is the instantaneous cylinder volume, and $V_{bowl}$ and $d_{bowl}$ are the piston bowl volume and diameter, respectively (Figure 3).

The mean velocity of the squish motion inside the cylinder, $U_{sq}$, is quantified by Equation 19 [21]. This velocity depends in turn on its axial, $U_a$, and radial, $U_r$, components that are related to main geometric characteristics of the cylinder and piston bowl and on the cylinder volume variation rate.

$$U_{sq} = \frac{1}{3}\left(U_r\left(1+\frac{d_{bowl}}{B}\right) + U_a\left(\frac{d_{bowl}}{B}\right)^2\right) \quad (19)$$

$$U_r = \frac{dV_{cyl}}{dt}\cdot\frac{V_{bowl}}{V\cdot\left(V_{cyl}-V_{bowl}\right)}\cdot\frac{B^2-d_{bowl}^2}{4d_{bowl}} \quad (20)$$

$$U_a = \frac{dV_{cyl}}{dt}\cdot\frac{s_{bowl}}{V} \quad (21)$$

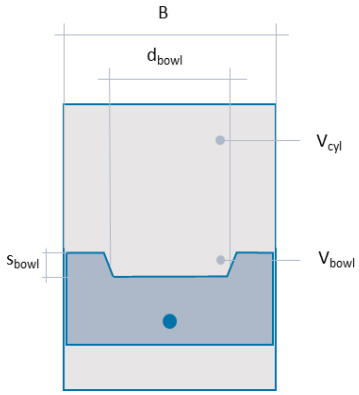


Figure 3 - Qualitative sketch of the main geometrical data of cylinder and piston.

**Production term** – This turbulence pattern belongs to the *K-k* model family. The energy cascade mechanism is modeled by the production term *P* (Equations 1-2) that is a subtractive quantity for the mean flow kinetic energy *K* and an additional term for the turbulent kinetic energy *k*. Since the piston and the walls of the combustion chamber do not allow to generate an ordered flow, during the first part of the intake stroke, the mean flow kinetic energy is much higher than the tumble and the swirl-associated kinetic energy. The tumble motion is low in this engine design, while the swirl motion is dominant. During the rising of the piston, the swirl vortex velocity increases due to angular momentum conservation, indeed the swirl radius is decreasing because of the flow motion entering the bowl. The shear stresses and internal viscous forces, because of the high swirl vortex velocity, cause the increasing of the turbulence kinetic energy near the TDC (Figure 4).

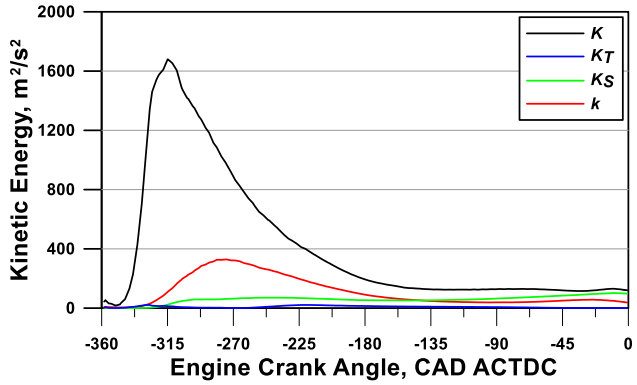


Figure 4 - Kinetic energies associated to mean, tumble, swirl and turbulent flows.

The turbulent production, caused by the tumble and swirl, is due the difference between the overall mean flow kinetic energy *K* and the ones associated to the two ordered flow motions: $K_T = U_T^2/2$ for the tumble and $K_S = U_S^2/2$ for the swirl (Equation 22).

$$P = c_{PKk} m \frac{K - K_T - K_S}{t_{TS}} \quad (22)$$

In the Equation above $c_{PKk}$ is a tuning constant to modulate the energy transfer from the mean flow to the turbulent one, $t_{TS}$ is a characteristic time scale determined by a weighted average that takes into account both tumble and swirl motions (Equations 23-24).

$$t_{TS} = w t_T + (1-w) t_S \quad (23)$$

$$w = \frac{|U_T|}{\sqrt{U_T^2 + U_S^2}} \quad (24)$$

**Dissipation term**

In the Equation 2, the dissipation rate $\varepsilon$ is determined through the Equation 25.

$$L_i = c_\mu^{3/4}\frac{k^{3/2}}{\varepsilon} \quad (25)$$

where $c_\mu$ is a constant and $L_i$ is the integral length scale. This last slightly differs according to the engine operating condition (speed, load, valve strategy, etc.), as it has been verified in other works [14], but manly depends on the engine type and the combustion chamber geometry. For this reason, the authors, in this *K-k-T-S* model, have chosen to impose $L_i$ evolution during the engine cycle according to a sequence of S-shaped functions. As shown below, the parameters of those functions are selected to fit $L_i$ trend derived from 3D simulations.

## 3D-CFD Setup

To calibrate the proposed 0-D turbulence model, 3D-CFD numerical simulations of the complete fluid exchange process were carried out on a CNG SI Heavy-Duty engine, whose main features are reported in Table 1. This power unit, derived from a Diesel CI engine, was operated under a variation of both speed and load to assess different flow and turbulence levels. Table 2 includes the most significant parameters of the two investigated operating conditions.

The 3D-CFD full cycle simulations were performed with Lib-ICE software, which is a code based on the OpenFOAM technology and extensively used for simulating IC engines for both academical and industrial tasks [16-18]. To accommodate the piston displacement and the valves motion, the *multiple mesh* technique was adopted [19, 20]. This consists in an automatic procedure: first, a Cartesian mesh is generated at the starting crank-angle; then it is deformed according to piston and valves motion through the resolution of a Laplace equation; finally the mesh quality is checked. When the mesh distortion is too high, a new Cartesian mesh is generated, and all computed fields are interpolated from the previous grid. Therefore, a

set of high-quality meshes, spanning from 0.4 to 3.4 mln. cells, allows the simulation of the whole fluid exchange process.

Table 1 - Main features of the selected CNG SI Heavy-Duty engine.

| Turbocharged SI Engine | |
|---|---|
| Cylinder Arrangement | 6l (in-line) vertical |
| Displacement, l | 12.85 |
| Compression Ratio | 12:1 |
| Stroke, mm | 150 mm |
| Bore, mm | 135 mm |
| Valves per cylinder | 4 |
| Bowl depth | ~30 mm |
| Bowl radius | ~37 mm |
| Average squish height | ~2.5 mm @ TDC |
| Maximum brake power, kW | 338 @ 1900 rpm |
| Maximum brake torque, Nm | 2000 @ 1100 / 1620 rpm |
| Injection System | MPI |
| Valve number | 4 |
| IVO – IVC at 2 mm lift, CAD AFTDC | 383-515 |
| EVO – EVC at 2 mm lift, CAD AFTDC | 146-333 |
| External EGR | NO |

Table 2 - The investigated operating conditions.

| Operating condition | *Cruise* | *Max power* |
|---|---|---|
| Engine speed [rpm] | 1200 | 1900 |
| Brake torque [Nm] | 850 | 1700 |
| Brake power [kW] | 100 | 338 |
| Normalized air-fuel ratio $\lambda$ | 1 | 1 |
| EGR [%] | 14.5 | 11.2 |

Governing equations were solved with the U-RANS approach and the $k$ - $\varepsilon$ model was chosen for turbulence. An overview of the investigated 3D-CFD domain is shown by Figure 5, where the selected piston is at TDC position. The unsteady effects of other cylinders, as well as intake and exhaust flow dynamics, are considered by imposing time-dependent pressure and temperature evolutions at both intake and exhaust patches (Figure 5). These boundary conditions were computed from 1-D simulations of the selected CNG engine, carried out with GT-Power software. The Natural Gas injection was simulated by imposing a constant mass flow rate of fuel at the PFI injector patch, in order to match the experimental values of: injection duration, end of injection (EOI) and $\lambda$ target inside the cylinder (Table 2).

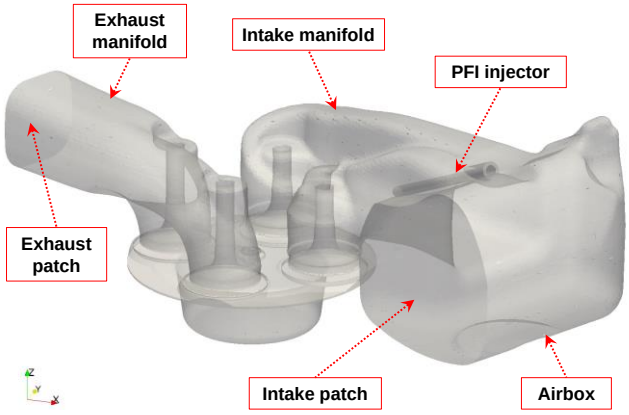


Figure 5 - Layout of the selected numerical domain for the 3D-CFD simulations, with the piston at the TDC position.

To get more insight on the organized flow motions (swirl, tumble and squish) affecting turbulence close to ignition event, the temporal evolution of the computed 3D fields of flow velocity $U$, turbulent kinetic energy $k$ and its dissipation rate $\varepsilon$ were analyzed during the compression stage over three different planes, whose position and orientation are reported in Figure 6.

The features of the computational grid employed to simulate the in-cylinder flow motion during the compression stroke are shown by Figure 7. An average cell size of 2 mm was selected inside the piston bowl during the whole engine cycle, as well as within the central region of the cylinder. This last choice was performed only when the piston position was far from TDC. Despite this dimension could be considered rather coarse, from author's experience it represents a good compromise between accuracy of results and low computational costs in modeling non-reacting flows inside wide regions of an heavy-duty engine cylinder. Then, a gradual refinement was introduced, in order to properly simulate the flow field in the squish region and around the cylinder head details (e.g.: spark-plug). Therefore, an average cell size of 0.5 mm was adopted between the piston and the cylinder head approaching the TDC, while a 0.25 mm average mesh dimension was employed to properly capture the spark-plug geometry and few details of the valves. Finally, a one-cell layer was included at the combustion chamber boundaries, in order to improve the prediction capabilities of the adopted scalable wall-functions.

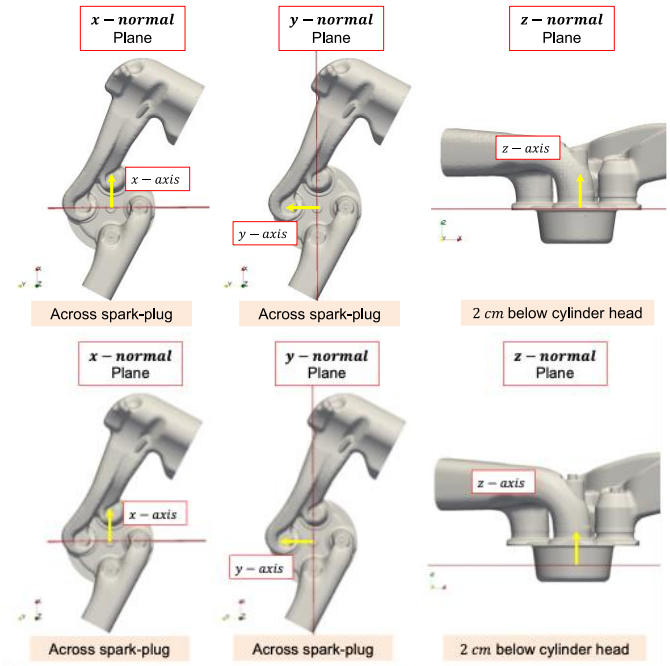


Figure 6 - Position of the three planes of investigation for *U*, *k* and *ε* distributions.

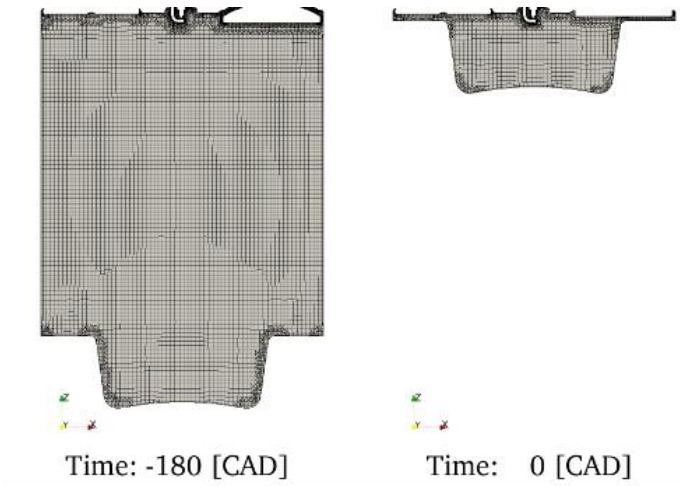


Figure 7 - The computational grid adopted inside the cylinder for the 3D-CFD simulations of the compression stroke: mesh features at the BDC (-180° ATDC) and the TDC (0° ATDC) on a y-normal plane (Figure 6).

Focusing on *Max Power* operating condition (Table 2) and comparing Figure 8, Figure 9, Figure 10 and Figure 11, at the end of the intake stage (-180° ATDC) it can be observed that the interaction of:

- several small tumble eddies (Figure 8 and Figure 9),
- two equi-rotating swirl eddies (Figure 10),

seem causing the average reduction of *U* and *k* observed in Figure 11. On the other hand, as the spark-advance is approached (-20° ATDC) two counter-interacting effects can be detected:

- A squish-generated flow interacts with the swirl motion inside the cylinder (Figure 8 and Figure 9). This is the cause of a high turbulence destruction near the squish region (Figure 8, Figure 9 and Figure 10).
- The swirl motion increases its intensity when it is “trapped” inside the cylinder bowl (conservation of the angular momentum, Figure 10). This generates an enhancement of the turbulence kinetic energy level inside the bowl (Figure 8, Figure 9 and Figure 10).

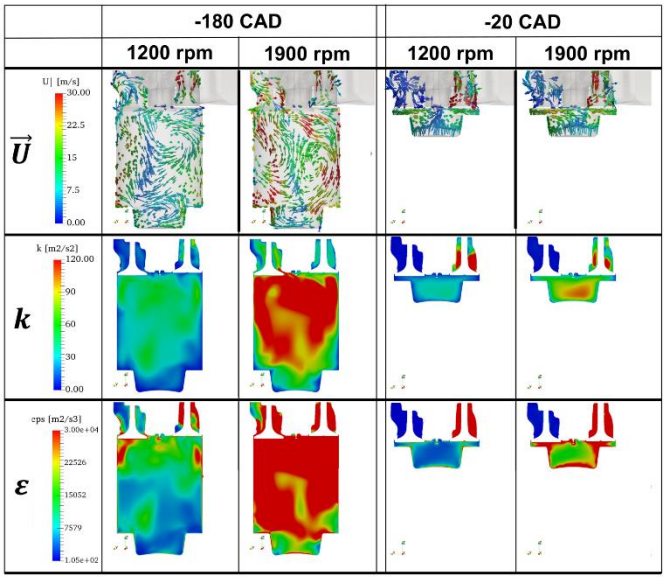


Figure 8 - Temporal evolution of *U*, *k* and *ε* fields on the x-normal plane (Figure 6) during compression stroke: from BDC (-180° ATDC) until around the spark-advance (-20° ATDC).

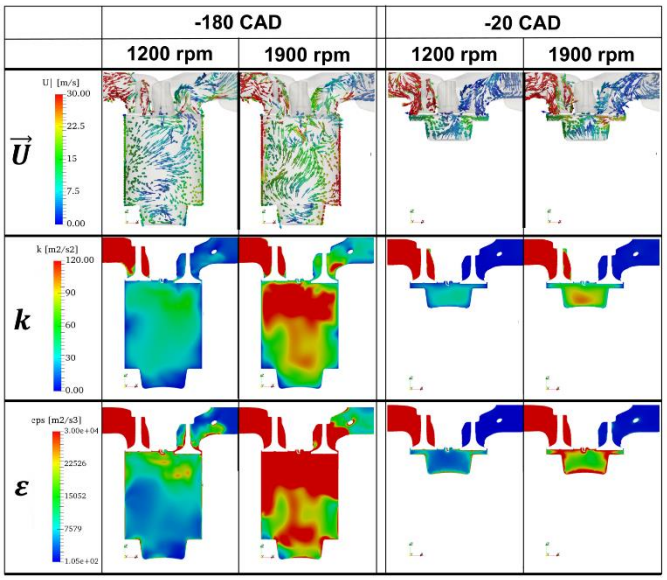


Figure 9 - Temporal evolution of *U*, *k* and *ε* fields on the y-normal plane (Figure 6) during compression stroke: from BDC (-180° ATDC) until around the spark-advance (-20° ATDC).

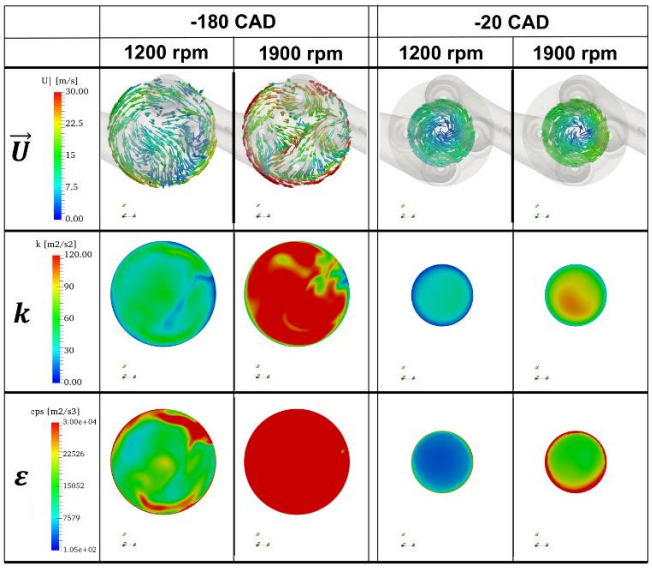


Figure 10 - Temporal evolution of $U$, $k$ and $\varepsilon$ fields on the z-normal plane (Figure 6) during compression stroke: from BDC (-180° ATDC) until around the spark-advance (-20° ATDC).

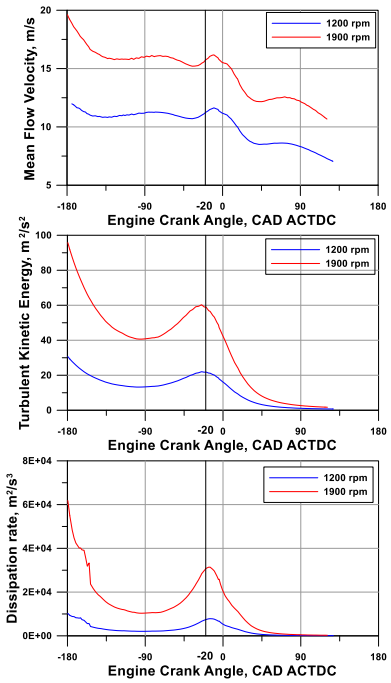


Figure 11 - Temporal evolution of computed $U$, $k$ and $\varepsilon$ values, averaged inside the cylinder during compression and expansion strokes of a motored engine cycle.

As a consequence, from Figure 11, it can be observed close to spark-advance (-20° ATDC):

- A net *increase* of the average $U$ and $k$ values when the "trapping" of the swirl motion inside the bowl is evolving and the squish motion is weak (*far* from TDC).
- A net *decrease* of the average $U$ and $k$ values when the "trapping" of the swirl motion inside the bowl is almost concluded and the squish motion is strong (*close* to TDC).

Similar conclusions can be drawn for the *Cruise* operating condition (Table 2), also if in presence of less intense $U$, $k$ and $\varepsilon$ fields (Figure 8, Figure 9, Figure 10 and Figure 11).

## Model tuning

The turbulence model includes ten tuning constants, namely:

- $c_{Kin0}$, acting on mean flow production during the intake stroke;
- $c_{Tin0}$, acting on tumble production during the intake stroke;
- $c_{fd0,T}$, defining the offset of the decay function for the tumble because of the viscous forces;
- $c_{fdm,T}$, adjusting the intensity of the tumble collapse near the TDC;
- $c_{PKk}$, adjusting the turbulence production from mean flow;
- $c_{Sin}$, acting on swirl production during the intake stroke (inlet);
- $c_{Sex}$, acting on swirl production during exhaust stroke (outlet);
- $c_{fd0,S}$, defining the offset of the decay function for the swirl because of the viscous forces;
- $c_{fdm,S}$, adjusting the intensity of the swirl/squish interaction before the TDC;

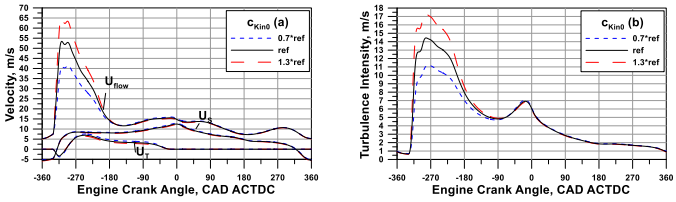


Figure 12 - $c_{Kin0}$ effect on mean flow, tumble and swirl velocities (a) and turbulence intensity (b).

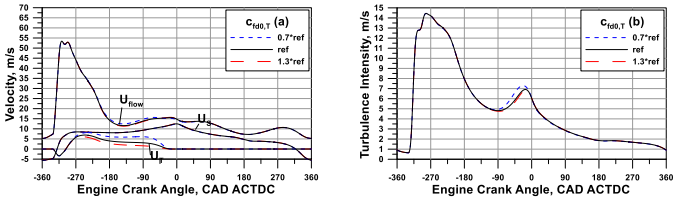


Figure 13 - $c_{fd0,T}$ effect on mean flow, tumble and swirl velocities (a) and turbulence intensity (b).

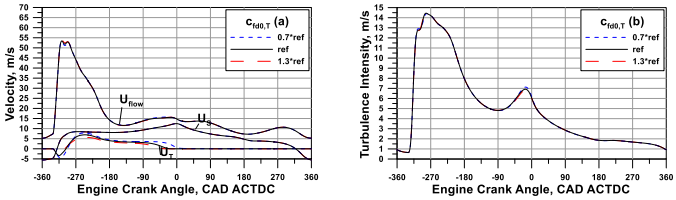


Figure 14 - $c_{fdm,T}$ effect on mean flow, tumble and swirl velocities (a) and turbulence intensity (b).

The Figure 12 - Figure 18 depict the effect of each tuning constant, by varying those from a reference value of ±30%. The impact on the mean flow, tumble and swirl velocities is highlighted on the left figures, while the turbulence intensity variations are plotted on the right ones. A parametric analysis has already been carried out by the authors, for completeness please refer to the previous work [15].

Figure 12 shows that $c_{Kin0}$ significantly modifies the mean flow and the turbulence peaks in the middle of the intake stroke, which

however turns in a reduced alteration of the turbulence speed-up, close to the TDC.

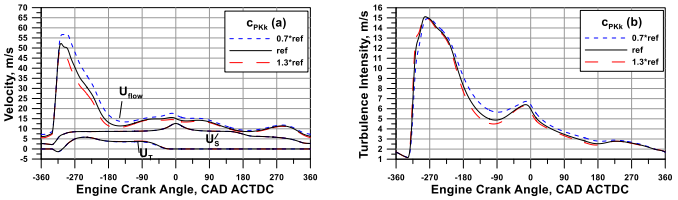


Figure 15 - $c_{PKk}$ effect on mean flow, tumble and swirl velocities (a) and turbulence intensity (b).

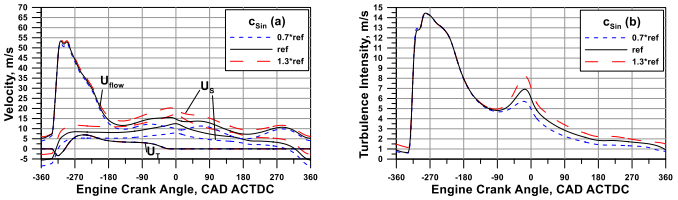


Figure 16 - $c_{Sin}$ effect on mean flow, tumble and swirl velocities (a) and turbulence intensity (b)

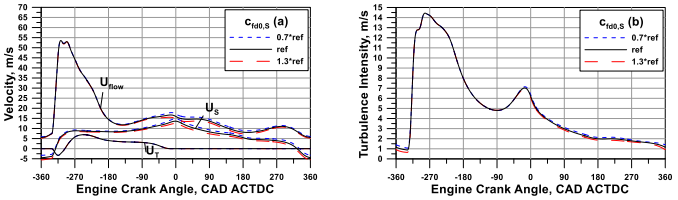


Figure 17 - $c_{fd0,S}$ effect on mean flow, tumble and swirl velocities (a) and turbulence intensity (b)

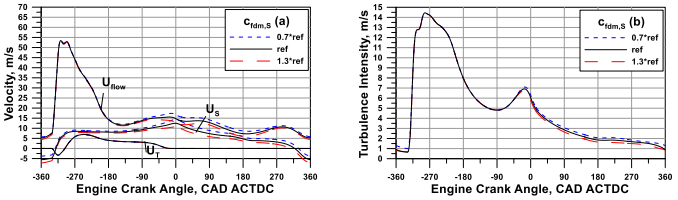


Figure 18 - $c_{fdm,S}$ effect on mean flow, tumble and swirl velocities (a) and turbulence intensity (b).

Figure 13 highlights that an increased (reduced) decay function offset, $c_{fd0,T}$, promotes (lowers) the decay of both mean flow and tumble velocities, turning in a less (more) intense turbulence production close to the TDC. The role of $c_{fdm,T}$ is shown in Figure 14. This underlines that this parameter controls the crank angle of the tumble collapse, with minor impact on the turbulence peaks. In Figure 15, the effect of $c_{PKk}$ is illustrated: this constant does not affect the tumble and swirl levels, while it modifies the turbulence trend during the compression stroke. It can be noted that a higher $c_{PKk}$ determines a lower turbulence during the compression, due to a lower $U$, although similar $u'$ peaks are reached before TDC.

Figure 16 shows the impact of $c_{Sin}$ on mean flow and swirl velocities. As expected, it promotes (lowers) the increasing (reducing) of swirl during the intake stroke, determining a higher (lower) initial velocity value. The generation of turbulence is given by the amount of kinetic energy in disordered form ($K$ - $K_T$ - $K_S$). Hence, despite of higher $U$ and $U_S$, the production of $u'$ in compression is not intense, then recovers to the TDC for the production term directly related to the swirl speed-up.

In the Figure 17 and Figure 18, the parameters that regulate the swirl decay function are presented. The figures highlight that the effects on mean flow and swirl velocity are qualitatively the same as the ones of tumble decay function. $c_{fd0,S}$ adjusts the swirl decay function offset, so it promotes (lowers) the decay of mean flow and swirl velocities during all cycle. $c_{fdm,S}$ controls the swirl decay around the TDC, adjusting its peak value.

Under the so far discussed sensitivity analysis, a tuning procedure can be advised. The primary step is matching the ordered flow of tumble and swirl with the 3D-derived results, adjusting firstly $c_{Tin0}$ and $c_{Sin}$. Secondly, $c_{Kin0}$ is identified to reproduce the 3D mean flow velocity peak during intake. The tumble collapse (the swirl peak) can be further handled by $c_{fd0,T}$ and $c_{fdm,T}$ ($c_{fd0,S}$ and $c_{fdm,S}$). The $c_{PKk}$ multiplier is fine-tuned to adjust the mean flow and turbulence trends, without a significant impact on the tumble and swirl levels and turbulence speed-up before TDC.

## Results and discussion

This section presents the predictions of the proposed 0D flow model at 2 operating conditions and compares them to the results obtained via 3D-CFD simulations. The operating conditions considered are at 1200 rpm and 1900 rpm at maximum load. The main features of the engine under study are reported in Table 1. It is a heavy-duty, turbocharged SI engine with a compression ratio of 12. The considered engine is retrofitted from a Compression Ignition (CI) application, through the installation of ported CNG injectors and spark-plugs. The CNG is injected through a Multi Point Injection (MPI) system, and it is metered to ensure a close-to-stochiometric air/fuel mixture in the combustion chamber. The load control is realized by the waste-gated turbocharger at mid/high load, and by the throttle valve at low load. An intercooler is located after the compressor to limit the inlet temperature of the air. Each cylinder is equipped with a centered spark-plug, and two intake and exhaust valves, both with a fixed timing.

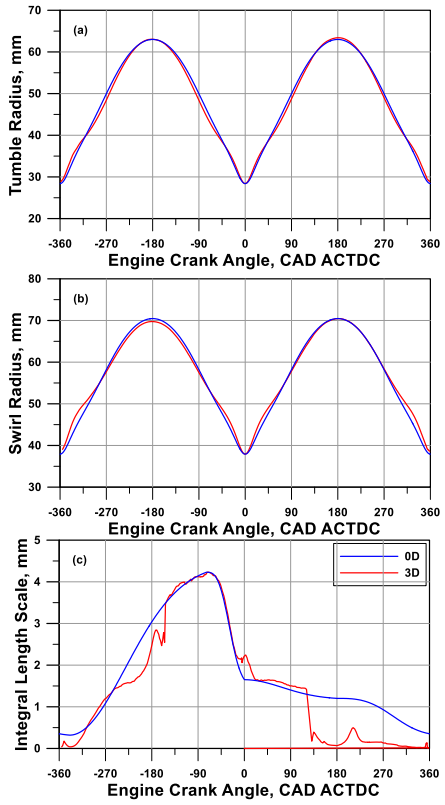


Figure 19 - Comparison between 3D-CFD and 0D results of tumble (a) and swirl (b) radii and integral length scale (c).

The first step in using the flow model is to calibrate the 0D model via the tuning constants, assuming ad reference 3D-CFD results. In the current study, the model was calibrated manually through a simple trial and error procedure to obtain a good match of all quantities of interest. The values obtained for the constants are listed in the Table 3. A mono-cylindrical 1D model of the engine under study is developed within a 0D/1D modeling environment, where the engine is schematized through a network of 1D pipes and 0D volumes. The 0D pattern is implemented as user sub-model using GT-Power tools and it ran in motored conditions just to evaluate the cold flow impact on turbulence generation, with no combustion influence.

As mentioned above in this *K-k-T-S* model, some data, more related to geometrical characteristics of the engine and combustion chamber, are not calculated, but imposed according to predefined patterns. The radii of tumble and swirl are calculated, through Equation 17, adjusting $c_{r0X}$ and $c_{rmX}$ parameters to match 3D levels at BDC and TDC, respectively. The integral length scale is calculated in a similar manner, assigning the levels at specific angular locations (firing TDC, minimum and maximum levels during intake and compression strokes, respectively). Figure 19 shows that the tumble and swirl radii are accurately matched by the 0D pattern during the whole engine cycle. The integral length scale is well reproduced, especially during the intake and compression strokes that are the phases more relevant for a reliable combustion prediction. 3D-CFD simulations highlighted no appreciable differences between the results of tumble/swirl radius and integral length scale for the two analyzed engine speeds, consequently presented 3D data refers only the case at 1900 rpm.

The values of the tuning constants were kept fixed for the operating conditions mentioned above with no case-dependent specific tuning.

Table 3 - Values of flow model tuning constants.

| Tuning constant | Value | Tuning constant | Value |
|---|---|---|---|
| $c_{Kin0}$ | 0.60 | $c_{Sin}$ | 0.08 |
| $c_{Tin0}$ | 0.45 | $c_{Sex}$ | 0.02 |
| $c_{fd0,T}$ | 0.55 | $c_{fd0,S}$ | 0.05 |
| $c_{fdm,T}$ | 1.0 | $c_{fdm,S}$ | 1.0 |
| $c_{PKk}$ | 3.5 | | |

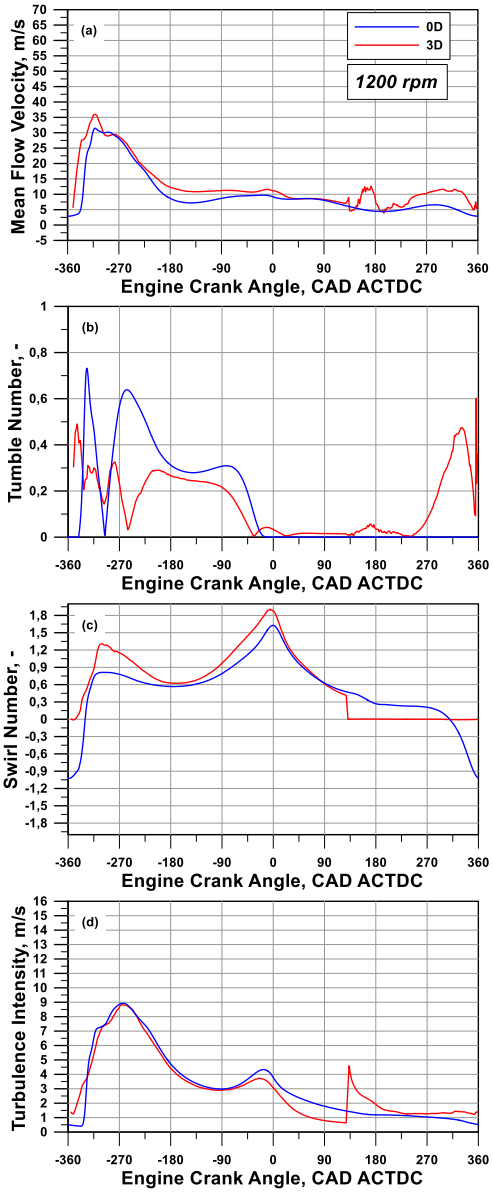


Figure 20 - Comparison between 3D-CFD and 0D results at 1200 rpm of mean flow velocity (a), tumble number (b), swirl number (c) and turbulence intensity (d).

Figure 20 and Figure 21 shows that the overall model behavior is quite satisfactory, since both the analyzed operating conditions are reproduced with good accuracy. The mean flow velocity, the tumble number, the swirl number and the turbulence intensity denote a very good agreement with the related 3D profiles, during each phase of the engine cycle. The *K-k-T-S* model considers the turbulence generation due to the disordered motion given by the difference between the mean flow kinetic energy with the tumble- and swirl-associated kinetic energies. The mean flow velocity increases at the TDC because of the swirl motion acceleration. The swirl radius reduces, approaching the TDC, due to the smaller volume available in the combustion chamber, so for the angular momentum conservation the swirl velocity enhances. The squish is not directly predicted, but its effects are indirectly taken into account as energy lost in the decay of the swirl. The turbulent intensity is satisfactorily predicted in the 0D pattern near to the TDC.

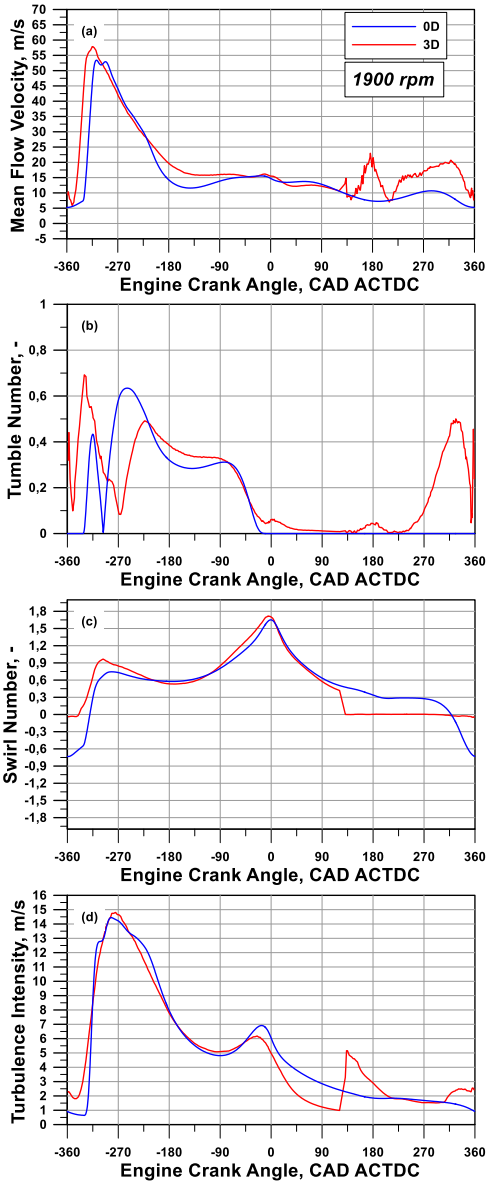


Figure 21 - Comparison between 3D-CFD and 0D results at 1900 rpm of mean flow velocity (a), tumble number (b), swirl number (c) and turbulence intensity (d).

As emerged from 3D analyses, tumble momentum presents components around x- and y-axes (Figure 6) having comparable intensities. Hence, for 0D model verification, those components are combined according to:

$$T_{XY} = \sqrt{T_X^2 + T_Y^2} \tag{25}$$

The overall tumble momentum is hence combined with tumble radius to derive the overall tumble number, plotted in Figure 20b and Figure 21b. For sake of consistency with 3D outcomes, the absolute value of the 0D predicted tumble number are considered for model validation. The tumble and swirl number profiles are satisfactorily reproduced during all engine cycle, with a higher accuracy towards the ending portion of the compression stroke, when the contribution of those motions to turbulence generation become more relevant. The model demonstrates to capture the global increase of *U* and *u'* levels when the engine rotational speed rises.

## Conclusions and future work

The present study introduces an improvement of a 0D phenomenological in-cylinder model based on a *K-k* approach already presented in a previous authors' work. The novelty of this model is the implementation of swirl as possible source for turbulence generation.

A parametric analysis, describing the role of each tuning constant, is presented with the aim of advising a tuning procedure. Once tuned, the model is tested for two different engine operating conditions. The predictions of this model are validated against results from 3D-CFD simulations under motored conditions.

The model involved nine tuning constants which were calibrated once for a single case, then the calibrated values were used unchanged for the other case.

Despite the difficulties in describing in a 0D pattern a complex 3D flow motion, the model quite well reproduces the mean flow, tumble, swirl and turbulence intensity profiles.

Future studies will involve to the implementation of this 0D pattern as sub-model for a combustion analysis, applied to the same engine.

## References


1. https://ec.europa.eu/clima/sites/clima/files/docs/pages/vision_1_emissions_en.pdf
2. Felix Leach, Gautam Kalghatgi, Richard Stone, Paul Miles, The scope for improving the efficiency and environmental impact of internal combustion engines, Transportation Engineering, Volume 1, 2020, 100005, ISSN 2666-691X, https://doi.org/10.1016/j.treng.2020.100005.
3. Alamia, A., Magnusson, I., Johnsson, F., & Thunman, H., "Well-to-wheel analysis of bio-methane via gasification, in heavy duty engines within the transport sector of the European Union." Applied energy, 2016, 170, 445-454, doi:10.1016/j.apenergy.2016.02.001
4. Blanco, H., Nijs, W., Ruf, J., Faaij, A., "Potential of Power-to-Methane in the EU energy transition to a low carbon system using cost optimization," Applied energy, 2018, 232, 323-340, doi:10.1016/j.apenergy.2018.08.027.
5. Wheeler, J., Stein, J., and Hunter, G., "Effects of Charge Motion, Compression Ratio, and Dilution on a Medium Duty Natural Gas

Single Cylinder Research Engine," SAE Int. J. Engines 7(4):1650-1664, 2014, doi:10.4271/2014-01-2363.
6. Johansson, B. and Olsson, K., "Combustion Chambers for Natural Gas SI Engines Part I: Fluid Flow and Combustion," SAE Tech. Pap. 950469, 1995, doi:10.4271/950469.
7. Heywood, J., B., "Internal combustion engine fundamentals," Vol. 930, New York, Mcgraw-Hill, 1988, ISBN: 007028637X.
8. Borgnakke, C., Arpaci, V., and Tabaczynski, R., "A Model for the Instantaneous Heat Transfer and Turbulence in a Spark Ignition Engine," SAE Technical Paper 800287, 1980, doi:10.4271/800287.
9. Morel, T. and Keribar, R., "A Model for Predicting Spatially and Time Resolved Convective Heat Transfer in Bowl-in-Piston Combustion Chambers," SAE Technical Paper 850204, 1985, doi:10.4271/850204.
10. Grasreiner, S., Neumann, J., Luttermann, C., Wensing, M. et al., "A Quasi-Dimensional Model of Turbulence and Global Charge Motion for Spark Ignition Engines with Fully Variable Valvetrains," International Journal of Engine Research 15(7):805-816, 2014, doi:10.1177/1468087414521615.
11. Fogla, N., Bybee, M., Mirzaeian, M., Millo, F. et al., "Development of a K-k-ε Phenomenological Model to Predict In-Cylinder Turbulence," SAE Int. J. Engines 10(2):562-575, 2017, doi:10.4271/2017-01-0542.
12. Bozza, F., De Bellis, V., Berni, F., D'Adamo, A. et al., "Refinement of a 0D Turbulence Model to Predict Tumble and Turbulent Intensity in SI Engines. Part I: 3D Analyses," SAE Technical Paper 2018-01-0850, 2018, doi:10.4271/2018-01-0850.
13. De Bellis, V., Bozza, F., Fontanesi, S., Severi, E. et al., "Development of a Phenomenological Turbulence Model through a Hierarchical 1D/3D Approach Applied to a VVA Turbocharged Engine," SAE Int. J. Engines 9(1):506-519, 2016, doi:10.4271/2016-01-0545.
14. Bozza, F., Teodosio, L., De Bellis, V., Fontanesi, S. et al., "Refinement of a 0D Turbulence Model to Predict Tumble and Turbulent Intensity in SI Engines. Part II: Model Concept, Validation and Discussion," SAE Technical Paper 2018-01-0856, 2018, doi:10.4271/2018-01-0856.
15. Bozza, F., Teodosio, L., De Bellis, V., Fontanesi, S. et al., "A Refined 0D Turbulence Model to Predict Tumble and Turbulence in SI Engines," SAE Int. J. Engines 12(1):2019, doi:10.4271/03-12-01-0002.
16. Paredi, D., Lucchini, T., D'Errico, G., Onorati, A. et al., "Gas Exchange and Injection Modeling of an Advanced Natural Gas Engine for Heavy Duty Applications," SAE Technical Paper 2017-24-0026, 2017, doi:10.4271/2017-24-0026.
17. Lucchini, T., D'Errico, G., Onorati, A., Bonandrini, G. et al., "Development and Application of a Computational Fluid Dynamics Methodology to Predict Fuel-Air Mixing and Sources of Soot Formation in Gasoline Direct Injection Engines," International Journal of Engine Research 15(5):581-596, 2014
18. Sforza, L., Lucchini, T., Gianetti, G., and D'Errico, G., "Development and Validation of SI Combustion Models for Natural-Gas Heavy-Duty Engines," SAE Technical Paper 2019-24-0096, 2019, doi:10.4271/2019-24-0096
19. Lucchini, T., Della Torre, A., D'Errico, G., Montenegro, G. et al., "Automatic Mesh Generation for CFD Simulations of Direct-Injection Engines," SAE Technical Paper 2015-01-0376, 2015, doi:10.4271/ 2015-01-0376
20. Lucchini, T., D'Errico, G., Paredi, D., Sforza, L. et al., "CFD Modeling of Gas Exchange, Fuel-Air Mixing and Combustion in Gasoline Direct-Injection Engines," SAE Technical Paper 2019-24-0095, 2019, doi:10.4271/2019-24-0095
21. Franken, T., Sommerhoff, A., Willems, W., Matrisciano, A. et al., "Advanced Predictive Diesel Combustion Simulation Using Turbulence Model and Stochastic Reactor Model," SAE Technical Paper 2017-01-0516, 2017, doi:10.4271/2017-01-0516.

## Contact Information

**M. Riccardi**, PhD Candidate (marco. riccardi@unina.it)
**V.De Bellis**, Associate Professor (vincenzo.debellis@unina.it),
**L. Sforza**, Researcher (lorenzo.sforza@polimi.it),
**C. Beatrice,** Researcher (c.beatrice@stems.cnr.it),
**F. Bozza**, Full Professor (fabio.bozza@unina.it),
**T. Lucchini**, Full Professor (tommaso.lucchini@polimi.it)
**V. Fraioli**, Researcher (valentina.fraioli@stems.cnr.it),
**M. Mirzaeian**, Performance Simulation team leader (mohsen.mirzaeian@cnhind.com),
**S. Langridge**, Leader - Thermo and Fluid Dynamics (Simon.langridge@cnhind.com),
**S. Golini**, Program Manager – Advanced Engineering (stefano.golini@cnhind.com)
CNR – STEMS, Via G. Marconi, 4, 80125 Naples, Italy
University of Naples "Federico II", Naples, Italy, +39-0817683264-3274
Polytechnic of Milano, via Lambruschini 4a, 20156 Milan, Italy
FPT Industrial S.p.A., Via Puglia 15, 10156 Turin, Italy
FPT Motorenforschung AG, Schlossgasse 2, 9320 Arbon, Switzerland

## Acronyms

| | |
|---|---|
| **0D/1D/3D** | Zero/One/Three–Dimensional |
| **ATDC** | After Top dead center |
| **CAD** | Crank angle degree |
| **CFD** | Computational Fluid Dynamics |
| **CI** | Compression Ignition |
| **CNG** | Compressed Natural Gas |
| **EOI** | End of Injection |
| **HD** | Heavy Duty |
| **ICE** | Internal Combustion Engine |
| **LNG** | Liquefied Natural Gas |
| **MPI** | Multi Point Injection |
| **PFI** | Port Fuel Injection |
| **PTG** | Power-to-Gas |
| **SI** | Spark ignition |
| **TCO** | Total Cost Ownership |
| **TDC** | Top Dead Center |
| **TKE** | Turbulent Kinetic Energy |

## Symbols

| | |
|---|---|
| $B$ | Cylinder bore |
| $B_\theta$ | Characteristic dimension of in-cylinder charge along radial direction |
| $c_{fd0,S}$, $c_{fdm,S}$ | Tuning constants of swirl decay function |
| $c_{fd0,T}$, $c_{fdm,T}$ | Tuning constants of tumble decay function |
| $c_{Kin0}$ | Tuning constant of inlet flow coefficient |
| $c_{PKk}$ | Tuning constant of turbulent production |
| $c_{r0,T}$, $c_{rm,T}$ | Parameters for tumble radius adjustment |
| $c_{r0,S}$, $c_{rm,S}$ | Parameters for swirl radius adjustment |
| $c_{Sin}$, $c_{Sex}$ | Tuning constants of swirl flow coefficient |
| $c_{Tin0}$ | Tuning constant of tumble flow coefficient |
| $d_{bowl}$ | Piston bowl diameter |
| $f_{d,S}$ | Decay function of swirl |
| $f_{d,T}$ | Decay function of tumble |
| $H$ | Piston position referred to cylinder head |
| $L_i$ | Integral Length Scale |
| $k$ | Turbulent kinetic energy |

| | |
|---|---|
| $K$ | Mean flow kinetic energy |
| $K_S$ | Kinetic energy related to swirl motion |
| $k_{sq}$ | Kinetic energy related to squish motion |
| $K_T$ | Kinetic energy related to tumble motion |
| $m$ | Mass |
| $N_{swirl}$ | Swirl number |
| $N_{tumble}$ | Tumble number |
| $P$ | Turbulence production |
| $r_S$ | Swirl radius |
| $r_T$ | Tumble radius |
| $s_{bowl}$ | Piston bowl height |
| $S$ | Swirl momentum |
| $t$ | Time |
| $t_S$ | Characteristic time scale of swirl |
| $t_T$ | Characteristic time scale of tumble |
| $t_{TS}$ | Weighted average characteristic time scale |
| $U$ | Mean flow velocity |
| $U_a$ | Axial mean flow velocity |
| $U_r$ | Radial mean flow velocity |
| $U_S$ | Swirl velocity |
| $U_{sq}$ | Squish velocity |
| $U_T$ | Tumble velocity |
| $v$ | Flow velocity throughout the valve |
| $V(\theta)$ | Instantaneous combustion chamber volume |
| $V_{cyl}$ | Cylinder volume |

## Greeks

| | |
|---|---|
| $\varepsilon$ | Dissipation rate |
| $\lambda$ | Relative air-to-fuel ratio |
| $\nu_t$ | Turbulent viscosity |
| $\rho$ | Density |
| $\omega$ | Angular velocity |

## Pedices

| | |
|---|---|
| $eng$ | Referred ti engine |
| $exb$ | Backward flow through the exhaust valve |
| $exf$ | Forward flow through the exhaust valve |
| $inb$ | Backward flow through the intake valve |
| $inc$ | Incoming flow inside the cylinder |
| $inf$ | Forward flow through the intake valve |
| $K$ | Related to mean flow kinetic energy |
| $out$ | Outcoming flow from the cylinder |
| $S$ | Related to swirl motion |
| $T$ | Related to tumble motion |

## Apices

| | |
|---|---|
| $\dot{}$ | Temporal derivative |